A STUDY OF THE FORMATION AND SCALING OF A SYNTHETIC JET

Final Report

Douglas R. Smith

Department of Mechanical Engineering
University of Wyoming
Laramie, WY 82070

31 March 2005

20050520 016

REPORT DOCUMENTATION PAGE

AFRL-SR-AR-TR-05-

0150

1. REPORT DATE (DD-MM-YYYY)	2. REPORT TYPE	3. DATES COVERED (From - To)
31032005	Finall Report	01 Apr 2001 - 31 Dec 2004

4. TITLE AND SUBTITLE	5a. CONTRACT NUMBER
A Study of the Formation and Scaling of a Synthetic Jet	
	5b. GRANT NUMBER
	F49620-01-1-0301
	5c. PROGRAM ELEMENT NUMBER

6. AUTHOR(S)	5d. PROJECT NUMBER
Douglas R. Smith	
	5e. TASK NUMBER
	5f. WORK UNIT NUMBER

7. PERFORMING ORGANIZATION NAME(S) AND ADDRESS(ES)	8. PERFORMING ORGANIZATION REPORT NUMBER
Department of Mechanical Engineering University of Wyoming Laramie WY 82070	

9. SPONSORING/MONITORING AGENCY NAME(S) AND ADDRESS(ES)	10. SPONSOR/MONITOR'S ACRONYM(S)
USAF/AFRL AFOSR 801 N. Randolph Street　NA Arlington VA 22203	AFOSR
	11. SPONSOR/MONITOR'S REPORT NUMBER(S)

12. DISTRIBUTION/AVAILABILITY STATEMENT

Distribution Statement A. Approved for public release; distribution is unlimited.

13. SUPPLEMENTARY NOTES

14. ABSTRACT
The broad goal of this study was to gain an improved understandiing for how synthetic jet actuators perform as flow control devices. This improved understanding is motivated by a need for enhancing and optimizing the design and operation of these devices for transition of the technology to larger scales.

To establish then a better understanding of how synthetic jets are formed and effect control, we undertook an experimental study with two objectives. The first objective was to study synthetic jet formation in a quiescent fluid environment. Here, we examined how the vortex ring formation parameters could be linked to the characteristics of the steady jet. Specific parameters of interest included the Reynolds number, a stroke length which is related to the frequency of the oscillatory motion at the orifice, and a geometric characteristic of the synthetic jet actuator, the orifice lip shape. The second objective was to examine the interaction of a synthetic jet with a cross-flow boundary layer. The intent here was to gain insight into how synthetic jets control a fundamental flow process, in this case, boundary layer separation. In addition, to examine how the cross-flow modifies the synthetic jet during

15. SUBJECT TERMS

16. SECURITY CLASSIFICATION OF:			17. LIMITATION OF ABSTRACT	18. NUMBER OF PAGES	19a. NAME OF RESPONSIBLE PERSON
a. REPORT	b. ABSTRACT	c. THIS PAGE			
U	U	U	UU	27	**19b. TELEPHONE NUMBER** (Include area code)

1 Introduction and Objectives

The broad goal of this study was to gain an improved understanding for how synthetic jet actuators perform as flow control devices. This improved understanding is motivated by a need for enhancing and optimizing the design and operation of these devices for transition of the technology to larger scales.

The term synthetic jet is generally used to describe the steady, turbulent flow that appears at some distance downstream of an orifice when an oscillating pressure gradient is applied across the orifice. Between the orifice, where the flow is purely oscillatory, and the point downstream, where an apparently steady jet exists, there exists one or more vortex rings. In the region of transition from an unsteady, periodic flow to a steady, turbulent flow, individual vortex rings are rapidly distorted by interactions with neighboring rings. The defining features of the vortex rings and how they interact with their neighbors are established during the time-periodic formation of the rings at the actuator orifice. These factors are also presumed to be closely linked to the defining characteristics of the ensuing steady, turbulent jet.

Past work has shown quite convincingly that synthetic jets are tremendously useful for controlling flow at scales much larger than the synthetic jet itself (Amitay et al. 2001; Smith and Glezer 2002). However, despite numerous demonstrations of synthetic jets in flow control applications, the mechanisms by which a synthetic jet effects control are still not well understood.

To establish then a better understanding of how synthetic jets are formed and effect control, we undertook an experimental study with two objectives. The first objective was to study synthetic jet formation in a quiescent fluid environment. Here, we examined how the vortex ring formation parameters could be linked to the characteristics of the steady jet. Specific parameters of interest included the Reynolds number, a stroke length which is related to the frequency of the oscillatory motion at the orifice, and a geometric characteristic of the synthetic jet actuator, the orifice lip shape. The second objective was to examine the interaction of a synthetic jet with a cross-flow boundary layer. The intent here was to gain insight into how synthetic jets control a fundamental flow process, in this case, boundary layer separation. In addition, to examine how the cross-flow modifies the synthetic jet during its formation, we studied the flow inside the actuator orifice and cavity. To gain access to this portion of the flow, a matched-index-of-refraction flow facility was used.

2 Experimental Approach

The experiments were performed in two facilities, one at the University of Wyoming (UW), and a second at Idaho National Engineering and Environment Laboratory (INEEL).

2.1 Experimental Setup: University of Wyoming

The UW experiments were performed in a 1.2 m × 1.2 m × 3.0 m water tank constructed of 3.8 cm thick Plexiglas. In units of the orifice diameter, D_o, the tank measures approximately $47D_o$

$\times$ 47D_o $\times$ 118D_o, and it can be assumed that the synthetic jet was operating in a quiescent environment of infinite extent.

The synthetic jet actuator was a piston-cylinder apparatus (Figure 1). The cylinder was 10.2 cm in diameter and 25.4 cm long. To permit optical access to the interior of the actuator cavity, the cylinder was also made of clear acrylic. The end of the cylinder was constructed of anodized aluminum with equally-spaced radial through-holes so that interchangeable face plates with various orifice lip geometries could be attached. The piston, was a solid Teflon cylinder fitted with two rubber gaskets to insure a water-tight fit. The piston was connected through a metal shaft to the carriage of a linear ball-screw slide. The motion of the slide was controlled by a computer-driven stepper motor that allowed for precise programming of the amplitude and frequency of the piston motion. The resolution of the stepper motor was 2000 steps per revolution and the resolution of the ball screw was 0.635 cm per revolution. This provided for an overall resolution of 3.175×10^{-8} cm/step.
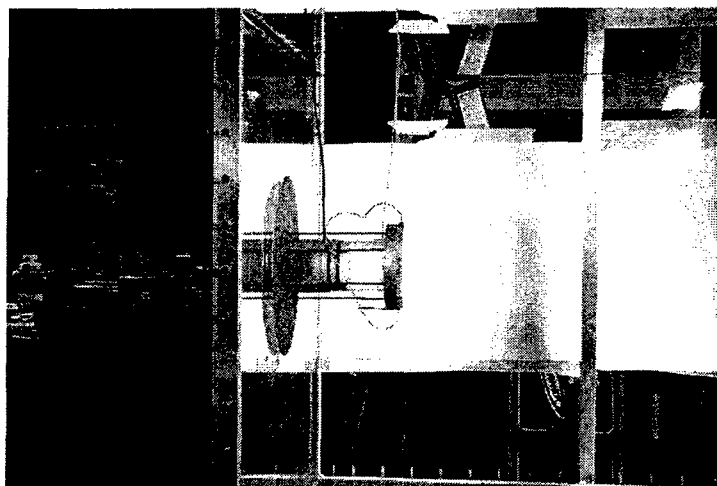

Figure 1: Water tank showing piston-cylinder synthetic jet actuator.

Three orifice lip geometries were studied: straight, beveled and rounded (Figure 2). The diameter of each orifice, D_o, was 2.54 cm, and the orifice depth, D_d, was 1.27 cm, or $D_d/D_o = 0.5$. An additional straight orifice was manufactured with a diameter of 0.74 cm and a depth of 3.68 cm, giving $D_d/D_o = 5$. Each orifice plate was constructed out of clear acrylic and was fabricated with small dye injection ports on the top and bottom of the orifice.

Two dimensional velocity field measurements were obtained using particle image velocimetry (PIV). The measurements were made in a plane that bisected the actuator orifice and jet flow-field. Phase-average and asynchronous measurements were obtained for the different jet flow fields. In the phase-averaged measurements, thirty-two vector fields were obtained at each of twenty-one phases across the period of the actuator forcing cycle. The asynchronous measurements were used to calculate a time-averaged flow field. For these measurements, 256 velocity vector fields were used to obtain mean flow-fields.
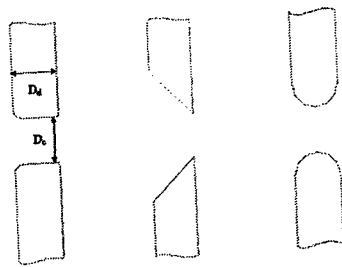
Figure 2: Orifice lip geometries.

2.2 Experimental Setup: INEEL

The synthetic jet in a cross-flow experiments were performed in the Idaho National Engineering and Environmental Laboratory (INEEL) Matched-Index-of-Refraction (MIR) flow facility (Figure 3). This facility uses a light mineral oil as the working fluid and quartz for the model material. The mineral oil and quartz have very nearly identical indices of refraction.

The INEEL-MIR facility consists of a settling chamber/flow conditioner, a contraction section, the test section, and a return loop. The settling chamber has an interior cross section of 1.22
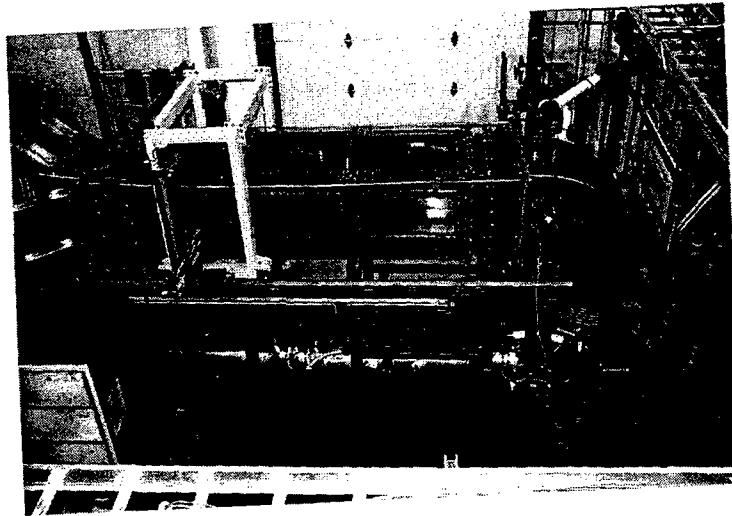
Figure 3: Flow facility at INEEL.

$\times$ 1.22 m and an overall length of 1.83 m. Flow conditioning is done with a honeycomb and three screens.

The contraction has an area ratio of 4:1, reducing the 1.22 x 1.22 m cross section to 0.61 x 0.61 m. The contraction has zero slope and curvature at the inlet and outlet and fifty per cent contraction at fifty per cent of its length. The contraction is symmetrical in the horizontal and vertical planes. A short entrance section of stainless steel connects the polycarbonate test section to the contraction.

The test section (Figure 3) is constructed of 3.8-cm (1-1/2 in.) thick polycarbonate plastic.

The inside dimensions of the test section are 0.61 m wide × 0.61 m high × 2.44 m long. For access to the inside of the test section, the top wall is constructed of three removable sections. Window inserts of soda-lime-float-glass are provided at three locations on the two vertical walls of the test section. These windows are about 63 cm long (24-3/4 in.) and 28 cm high (11 in.) with a thickness of 1.9 cm (3/4 in.).

The axial flow pump provides a maximum flow rate of 340 liters/sec (5400 gpm) at about three meters (10 feet) water head. This maximum flow rate corresponds to a maximum test section velocity of 0.9 m/s. However, with an empty test section, velocities of about 1.7 m/sec have been measured at 500 rpm. The pump has four blades and is driven by a 75 hp motor in conjunction with a variable frequency controller.

The cross-flow model was constructed of aluminum and polished quartz and was suspended in the test section. The model consisted of four 1.27 cm thick plates which span nearly the entire width of the test section. The first plate had a leading edge shaped like a NACA 0009 symmetric airfoil. The first, second and fourth plates were all constructed of aluminum, while the third plate was constructed of polished quartz. A 2.54 cm polished straight hole was located in the center of this plate. Centered about this hole was a quartz cylinder with an inner diameter of 10.2 cm and a 0.64 cm wall thickness (Figure 4). For the inclined orifice studies, a 2.54 cm orifice was machined in the plate with its axis inclined at 30° (relative to the vertical) in the downstream direction. The same piston and linear slide apparatus that was used in the University of Wyoming experiments was also used in these experiments.
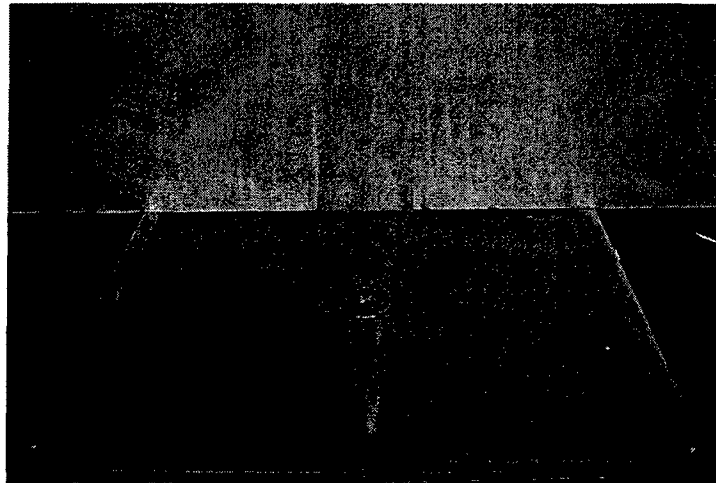

Figure 4: Photograph of quartz plate and cylinder.

2.3 Theoretical Background: Slug Flow Model for Vortex Ring Formation

By analogy with the formation of vortex rings in isolation, a slug flow model (Glezer 1988) was adopted to identify the important formation parameters for the synthetic jet. In this model, the fluid is ejected from the orifice as a cylindrical slug with length, L_o, and diameter, D_o. The slug length is identified with the stroke of the oscillatory motion at the orifice and can be

obtained from the time-varying velocity at the orifice by

$$L_o = \int_0^{T/2} u(t)\, dt$$

where T is the period of the oscillatory motion and u(t) is the velocity at the orifice exit. A velocity, U_o, can then be obtained from the stroke by

$$U_o = \frac{L_o}{T}$$

This velocity is used to define a Reynolds number, Re_{U_o}, according to

$$Re_{U_o} = \frac{U_o D_o}{\nu}$$

The shape of the velocity profile is characterized by a program factor, P, and defined as

$$P = \frac{U_o^2}{\overline{U_o^2}}$$

where

$$\overline{U_o^2} = \frac{1}{T} \int_0^{T/2} u^2(t)\, dt$$

In this study, the actuator was driven with a sinusoidal forcing for which $P \approx 1.27$; P takes a value of unity for a square wave program.

3   University of Wyoming Experimental Results

Extensive phase-averaged and time-averaged data sets were obtained for the synthetic jet flow-fields in a quiescent fluid. Table 1 identifies the stroke and Reynolds number combinations for the phase-averaged measurements obtained in the UW experiments.

3.1   Vorticity Contours from Phase-averaged PIV Measurements

To determine the conditions when one or more vortex rings exists between the orifice and the synthetic jet, vorticity contours were examined at two phase angles during the actuator cycle: 126° and 234°, corresponding to points during the expulsion and suction, respectively.

Figure 5 shows vorticity contours with an overlay of velocity vectors for the straight orifice at three values of L_o/D_o and Re_{U_o}=2500. Similar figures (not shown) for the beveled and round orifice exhibit similar trends. The formation vortex ring is clearly identifiable by high concentrations of positive and negative vorticity. At L_o/D_o=1 (Figure 5a), only one complete coherent ring is visible; however, for L_o/D_o=2 and 3 (Figures 5c and 5e), a second ring, formed during the previous actuator cycle, is also visible. At L_o/D_o=1, the formation vortex ring breaks down close to the orifice, and a synthetic jet is apparent within one diameter of the orifice. In each subfigure, the streamwise distance is scaled on L_o, and it appears that the position of the formation vortex ring during the actuator cycle scales approximately with x/L_o.
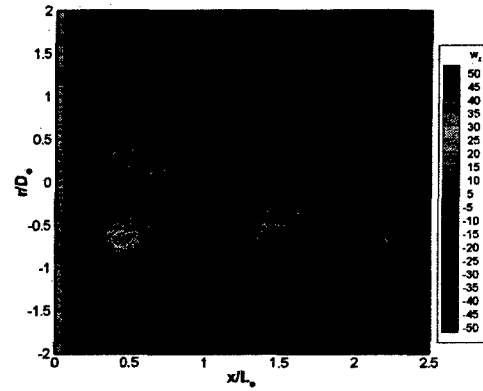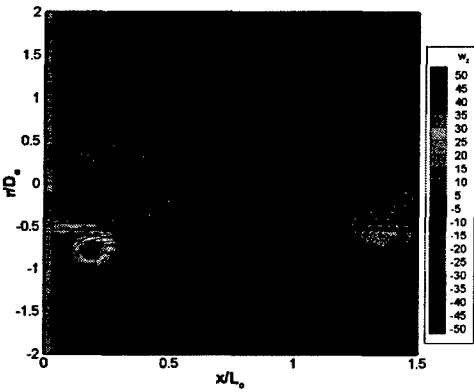
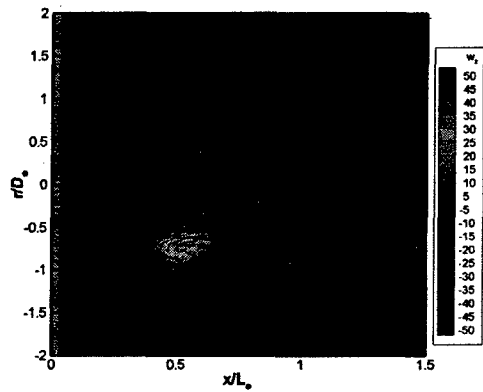(a) L_o/D_o=1, ϕ=126°.

(b) L_o/D_o=1, ϕ=234°.

(c) L_o/D_o=2, ϕ=126°.

(d) L_o/D_o=2, ϕ=234°.

(e) L_o/D_o=3, ϕ=126°.
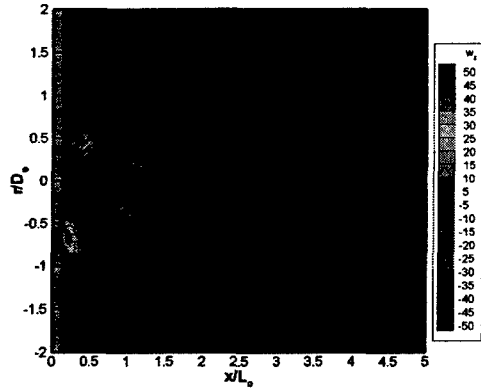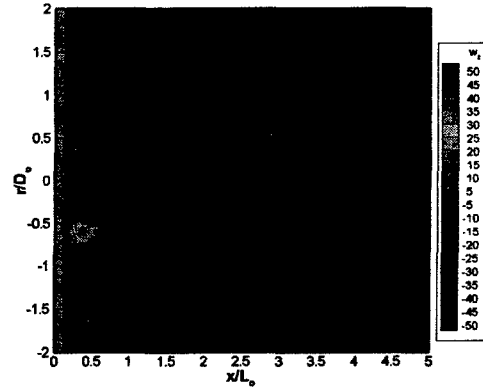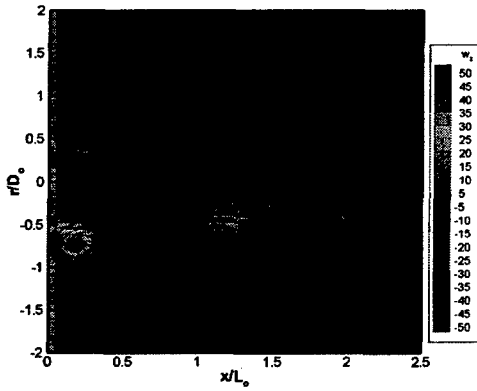
(f) L_o/D_o=3, ϕ=234°.

Figure 5: Contours of vorticity, ω_z, with velocity overlay for the straight orifice. $Re_{U_o} = 2500$.

6

L_o/D_o	Re_{U_o}	Straight	Beveled	Round	Small
0.2	500		•		
0.4	1000		•		
0.6	2500		•		
1	1000	•	•	•	•
1	2500	•	•	•	
1	5000	•	•	•	
2	1000				•
2	2500	•	•	•	
3	1000				•
3	2500	•	•	•	•
3	5000	•	•	•	
3	10000	•	•	•	

Table 1: Summary of conditions for which phase-averaged measurements were obtained in the UW experiments.

Figure 6 shows vorticity contours with an overlay of velocity vectors for the straight orifice at three values of Re_{U_o} and $L_o/D_o=3$. These figures show that an increase in Reynolds number increases the strength of the circulation associated with each ring, but does not affect the location of the vortex ring during the actuator cycle, nor does it appear to affect the position where the vortex rings begin to undergo distortion in the transition to a synthetic jet.

A comparison of the flow-fields for the straight, beveled and round orifices at the same stroke and Reynolds number, 2.0 and 2500, respectively, are shown in Figure 7. At the expulsion phase angle ($\phi = 126°$), two vortex rings are visible in each flow-field, although the positions of the rings are different for the different orifices. Comparing the straight and beveled orifices, the forming vortex ring is at approximately the same scaled streamwise location; however, the ring formed at the beveled orifice during the previous actuator cycle has convected farther downstream than the corresponding ring from the straight orifice. The ring forming at the round orifice is closer to the face of the orifice plate, because the separated shear layers that form the vortex ring originate midway between the front and back faces of the orifice plate; whereas, for the straight and beveled orifices, the shear layers separate at the orifice lip on the front face of the orifice plate. Despite initially forming closer to the orifice plate, the vortex ring formed at the round orifice during the previous actuator cycle is at approximately the same location as the corresponding vortex ring from the straight orifice, indicating a higher convection velocity after the formation is complete.
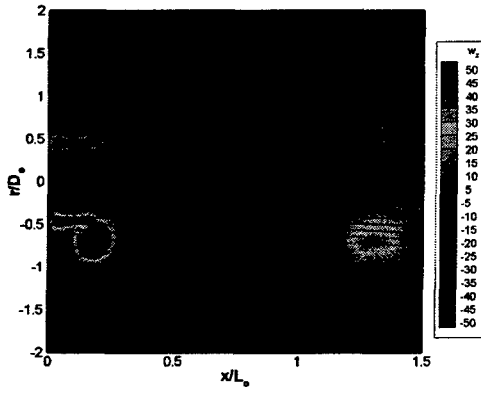
3.2 Vortex Ring Trajectories

It is apparent from Figures 5-7 that the position of the formation vortex ring during the actuator cycle depends on the stroke and the shape of the orifice lip. To examine in greater detail this dependence, the location of the vortex rings was mapped in time for approximately one actuator cycle.
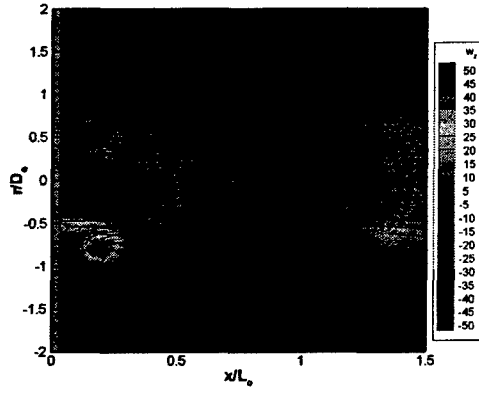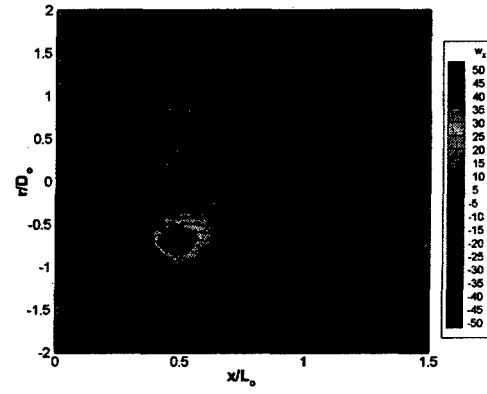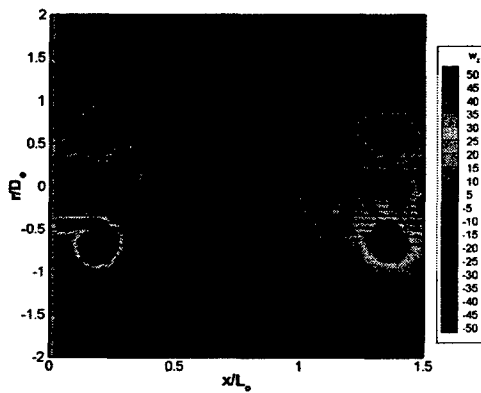
(a) $\mathrm{Re}_{U_o}=2500$, $\phi=126°$.
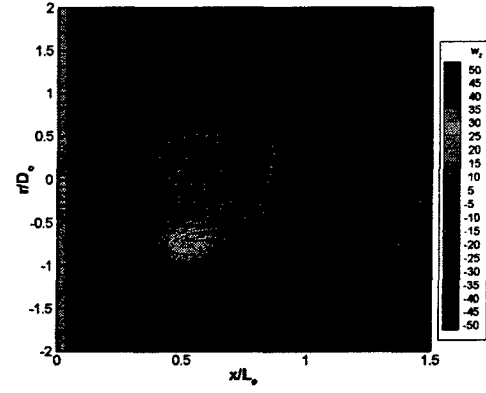
(b) $\mathrm{Re}_{U_o}=2500$, $\phi=234°$.

(c) $\mathrm{Re}_{U_o}=5000$, $\phi=126°$.
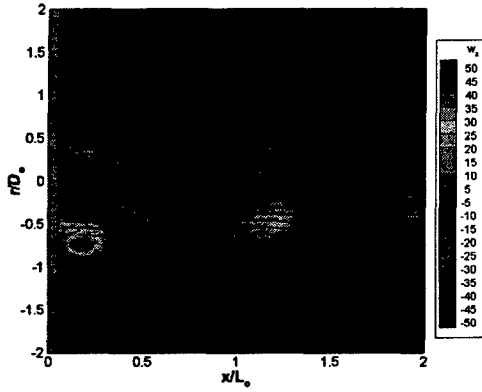
(d) $\mathrm{Re}_{U_o}=5000$ $\phi=234°$.
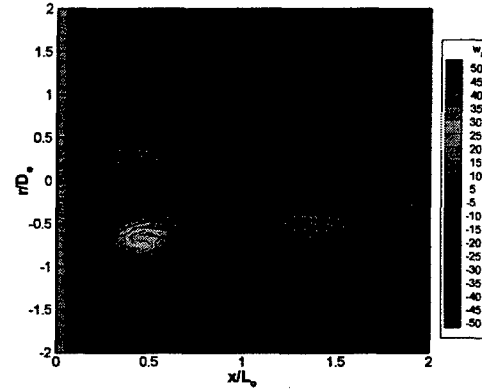
(e) $\mathrm{Re}_{U_o}=10000$, $\phi=126°$.
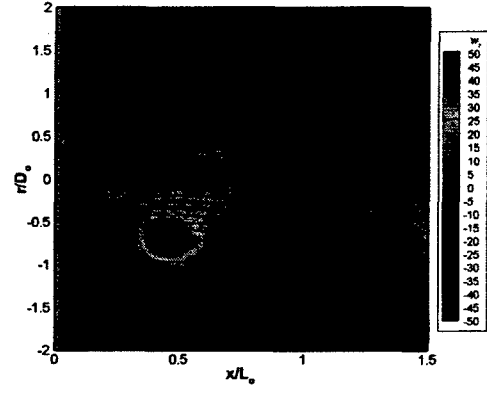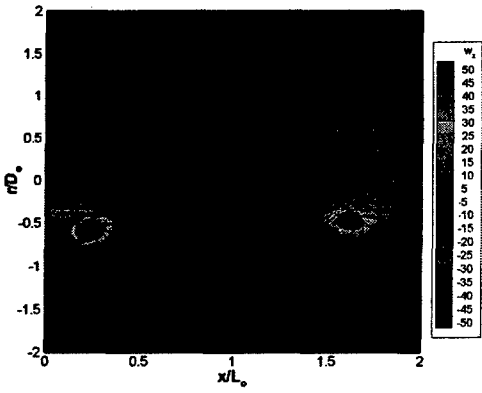
(f) $\mathrm{Re}_{U_o}=10000$ $\phi=234°$.

Figure 6: Contours of vorticity, ω_z, with velocity overlay for the straight orifice. $L_o/D_o=3$.
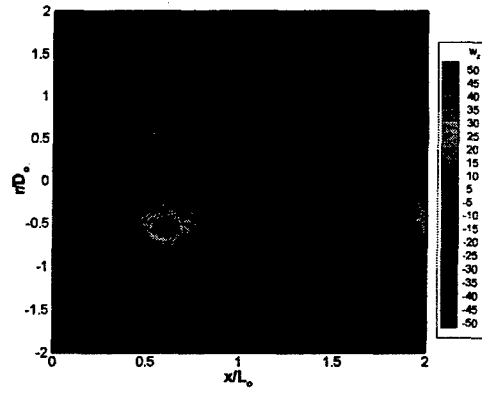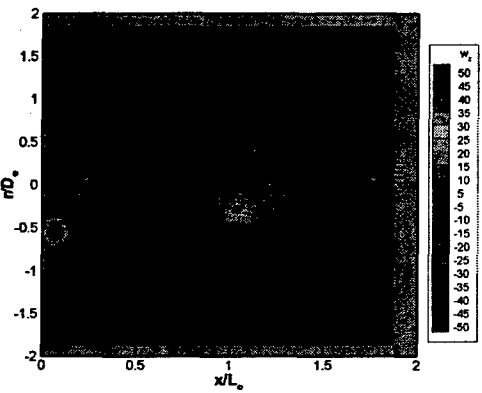
8

(a) Straight orifice. $\phi=126°$.

(b) Straight orifice. $\phi=234°$.

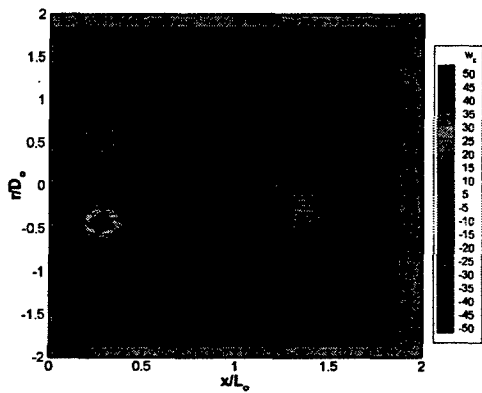(c) Beveled orifice. $\phi=126°$.

(d) Beveled orifice. $\phi=234°$.

(e) Round orifice. $\phi=126°$.

(f) Round orifice. $\phi=234°$.

Figure 7: Comparison of vorticity contours, ω_z, with velocity overlay for the straight, beveled and round orifices. $L_o/D_o = 2$, $Re_{U_o} = 2500$.

Figure 8 shows the convection of the formation vortex ring for the straight orifice at three values of L_o/D_o and $Re_{U_o}=2500$. At $L_o/D_o=1$, the formation vortex ring convects downstream during the expulsion phase, reaching $x/L_o \approx 0.4$ by the end of this phase. During the suction phase of the cycle, the forward motion of the ring is retarded, and the ring does not convect beyond $x/L_o \approx 0.6$ by the end of the actuator cycle. As the next cycle begins, the next vortex ring interacts with this existing ring, distorting it and leading to the formation of a synthetic jet. In contrast, for $L_o/D_o=2$ and 3, the formation vortex rings follow an approximately linear trajectory. The trajectories of the rings for $L_o/D_o=2$ and 3 overlap until $t/T \approx 0.48$ and $x/L_o \approx 0.3$ at which point the two trajectories begin to diverge. As this divergence begins at the mid-point of the actuator cycle ($t/T=0.5$), it is reasonable to attribute it to an effect from the suction phase of the actuator. The above observations suggest an increase in the actuator stroke acts to diminish the effect of the suction phase on the formation vortex ring, and thus increase the distance travelled by the ring before it begins undergo distortion leading to a synthetic jet. Similar results were reported by Smith et al. (1999).
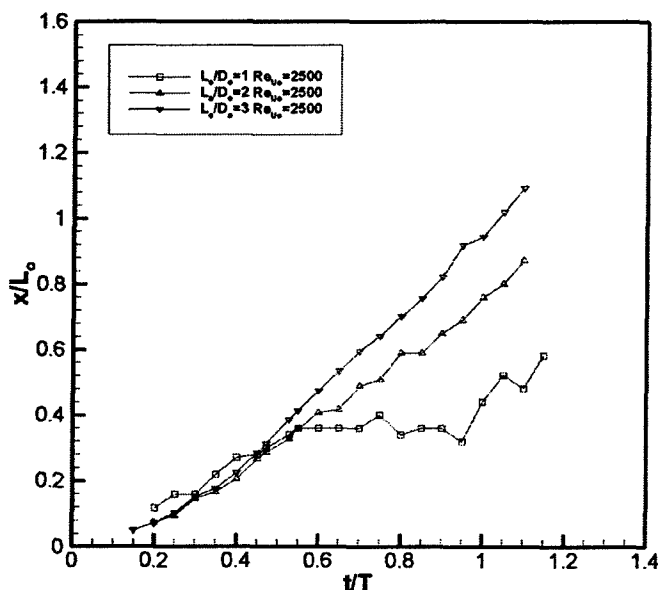

Figure 8: Convection of a vortex ring for the straight orifice. $Re_{U_o}=2500$ and varying L_o/D_o.

Figure 9 shows the formation vortex ring trajectories for the straight orifice at three values of Re_{U_o} and $L_o/D_o=3$. Here, we observe that the convection velocity of the vortex rings increases during the formation of the ring, but reaches a constant value by the end of the expulsion phase that does not change with increasing Reynolds number.

A comparison of the vortex ring trajectories for the straight, beveled and round orifices at $Re_{U_o}=2500$ and $L_o/D_o=3$ is shown in Figure 10. For both the straight and beveled orifices, the forming vortex ring begins its motion at approximately the same position in space and time. For the round orifice, however, the forming vortex ring does not appear until much later in
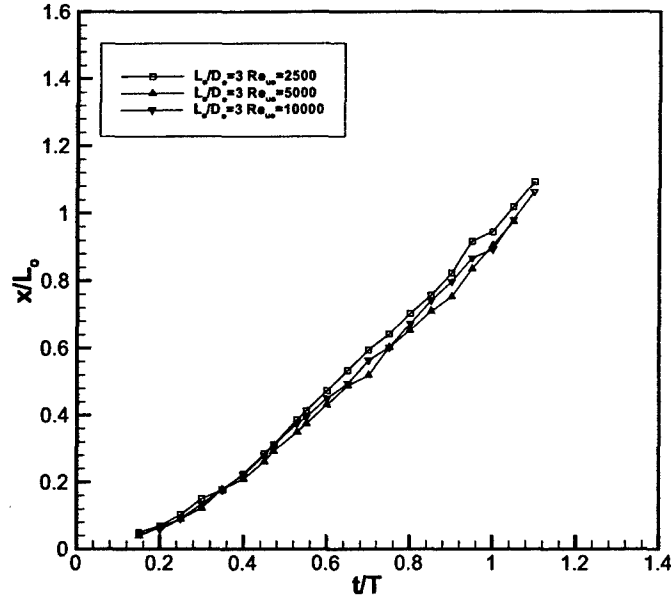
10

Figure 9: Convection of a vortex ring for the straight orifice. Varying Re_{U_o} for $L_o/D_o = 3$.

time. This later entry of the formation ring for the round orifice can be attributed to the fact that the vortex ring formation begins at a point midway between the front and back faces of the orifice plate. The slopes of the ring trajectories for the straight and the round orifices are approximately equal for $x/L_o > 0.4$ with the slope for the beveled orifice slightly steeper.

A shallower slope and slower convection velocity would indicate that the formation ring for the straight orifice is more likely to be affected by the suction phase than the formation ring from the beveled orifice. It would seem then that this larger velocity could be an explanation for why the rings from the beveled orifice remain coherent at non-dimensional strokes that cause the rings from the straight orifice to break down. If the non-dimensional velocity of the rings, however, was the only parameter of indication for the creation of a jet, then a jet should be present at $L_o/D_o = 1$ for the round orifice since the non-dimensional velocities of the round and the straight orifices are essential equal. This, however, is not observed. A better criteria for the formation of a jet would be the position of a vortex ring at a certain time in the formation cycle.

3.3 Time-averaged PIV Results

Time-averaged measurements were obtained asynchronously to the actuator forcing frequency to provide mean flow fields that illustrate how changes in the stroke, Reynolds number, and orifice lip shape affect the flow in the mean.
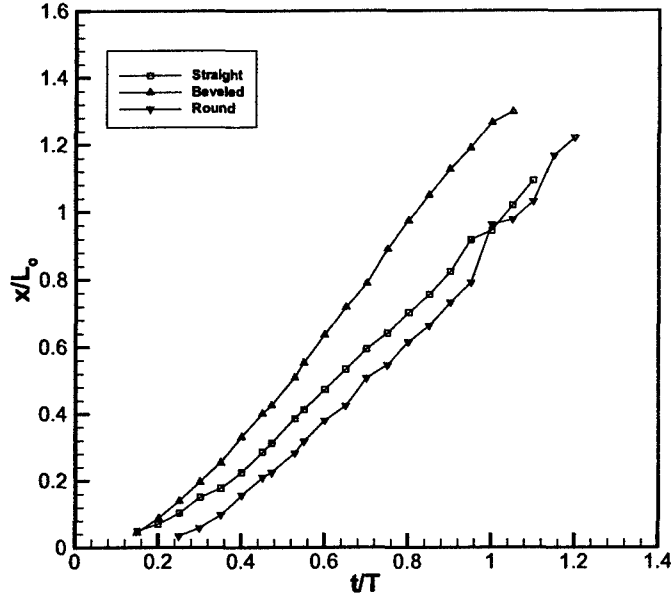
11

Figure 10: Comparison of the convection of a vortex ring for the straight, beveled and round orifice. Re_{U_o}=2500 and L_o/D_o=3.

3.3.1 Centerline Velocity Variation

Figure 11 shows the streamwise variation of the velocity along the centerline of the mean flow for the straight orifice. The streamwise variation for three values of L_o/D_o at Re_{U_o}=2500 are shown. The general trend for the centerline mean velocity is to increase from zero at the orifice to a peak at $x \approx L_o$ then decrease with increasing streamwise distance. At this Reynolds number, the streamwise position where the mean centerline velocity peaks occurs at the same value of x/L_o for the three values of L_o/D_o. This trend was observed for the beveled and round orifices; however, the x/L_o location where the centerline velocity reaches a peak was different for the different orifice shapes.

Figure 12 shows the streamwise variation in the centerline velocity for the straight orifice at three values of Re_{U_o} and L_o/D_o=2. Except for the data at Re_{U_o} = 1000, the streamwise variations all collapse. Note that here the streamwise distance, x, is scaled on D_o.

A comparison of the streamwise variation in the centerline velocity for the straight, beveled, and round orifice at two values of L_o/D_o and Re_{U_o}=2500 is shown in Figure 13. At L_o/D_o=2 (Figure 13a), the peak values of the centerline velocity for the straight and the beveled orifices are approximately the same; however, the centerline velocity for the beveled orifice peaks farther downstream. At this value of the stroke, the streamwise velocity variations for both the straight and the round orifices are similar but with differing magnitudes. The velocity variation for the beveled orifice exhibits a sustained and nearly constant value until x/D_o=6 where a rapid but modest descrease occurs before leveling off farther downstream. Clearly, the coherence of the
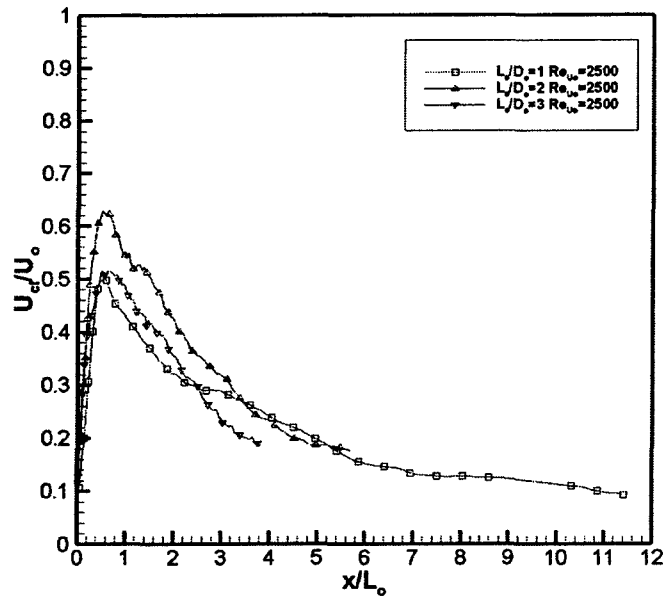
12

Figure 11: Centerline velocity variation for the straight orifice. Constant Re_{U_o} and varying L_o/D_o.
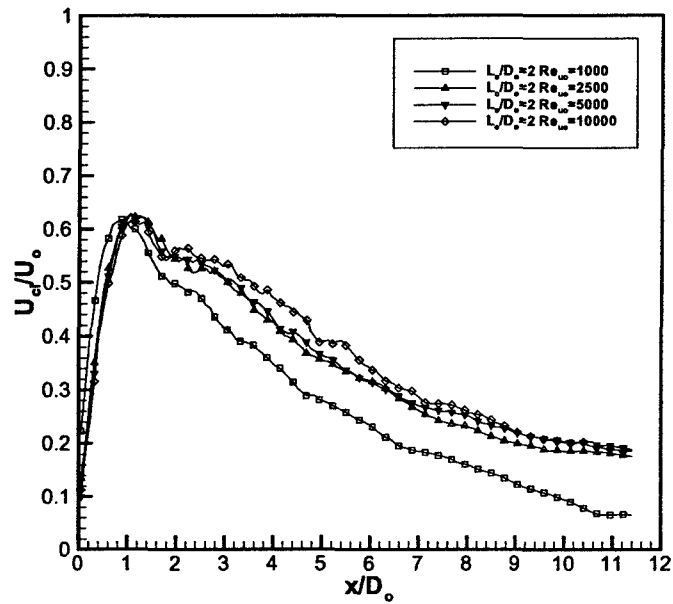

Figure 12: Centerline velocity variation for the straight orifice. Constant $L_o/D_o=2$ and varying Re_{U_o}.

13

vortex rings from the beveled orifice influences the mean flow-field.

At $L_o/D_o=3$ (Figure 13b), the velocity variations for the straight and the beveled orifices once again peak at approximately the same value. At $L_o/D_o=2$, the trends in the centerline velocity are similar for the straight and the round orifices; however, at $L_o/D_o=3$, it is the beveled and the round orifices profiles that have similar trends. This observation would indicate that a change in the stroke has a greater affect on the coherency of the vortex rings for the round orifice than for either the straight or beveled orifices.
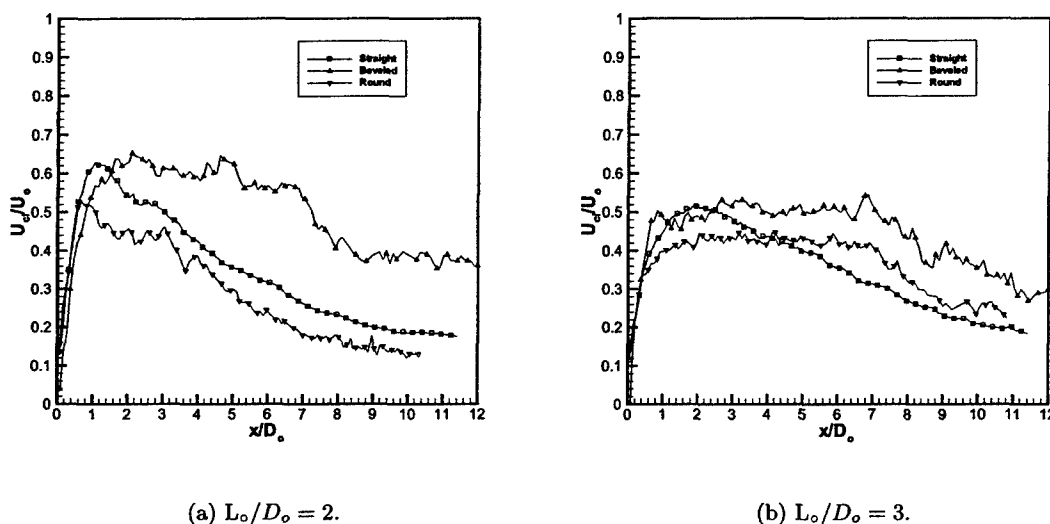

(a) $L_o/D_o = 2$.   (b) $L_o/D_o = 3$.

Figure 13: Comparison of the centerline velocity variation for the straight, beveled and round orifice. Constant L_o/D_o and $Re_{U_o}=2500$.

3.3.2 Jet Width

At any streamwise location, the width of the mean flow, b, can be defined as the sum of the distances above and below the jet centerline where the mean streamwise velocity has fallen to one-half the peak centerline value. Figure 14 shows the streamwise variation in the non-dimensional width, b/D_o, for the straight orifice at three values of L_o/D_o and $Re_{U_o}=5000$. This figure shows that for a constant Re_{U_o}, the location where the jet first begins to grow scales on L_o and consistently begins at $x \approx L_o$. This figure also shows that as L_o/D_o increases the initial width of the jet increases and the rate, in terms of x/L_o, at which the jet grows increases.

Figure 15 shows the streamwise variation in the mean flow width for the straight orifice at four values of Re_{U_o} and $L_o/D_o=3$. The streamwise variation in the non-dimensional width is approximately invariant with Reynolds number.

A comparison of the mean flow width for the straight, beveled and round orifices at two values of L_o/D_o for $Re_{U_o}=2500$ is shown in Figure 16. For $L_o/D_o=2$ (Figure 16a), the growth of the
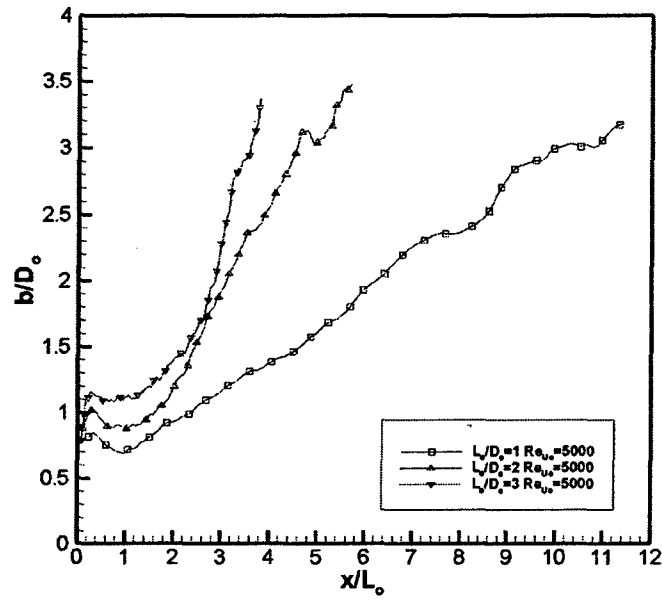
14

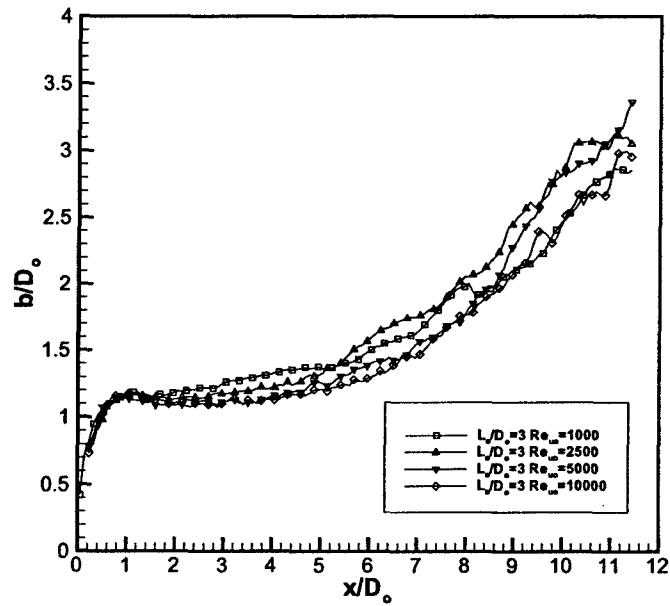Figure 14: Jet width for the straight orifice. Constant Re_{U_o}=5000 and varying $\mathrm{L_o}/D_o$.

Figure 15: Jet width for the straight orifice. Constant $\mathrm{L_o}/D_o$=3 and varying Re_{U_o}.

15

jet for the straight orifice begins at approximately $x/D_o=2$, while the growth for the round and the beveled orifices begin at approximately $x/D_o=3.5$ and 6, respectively. At $L_o/D_o=3$ (Figure 16b), the growth of the jet for the straight orifice begins at approximately $x/D_o=5$, while the round and the beveled jet begin growing at approximately $x/D_o=6$ and 8, respectively. This trend indicates that the starting location of the increase in the jet width is more affected by L_o/D_o at these conditions for the round orifice than for the straight or the beveled.
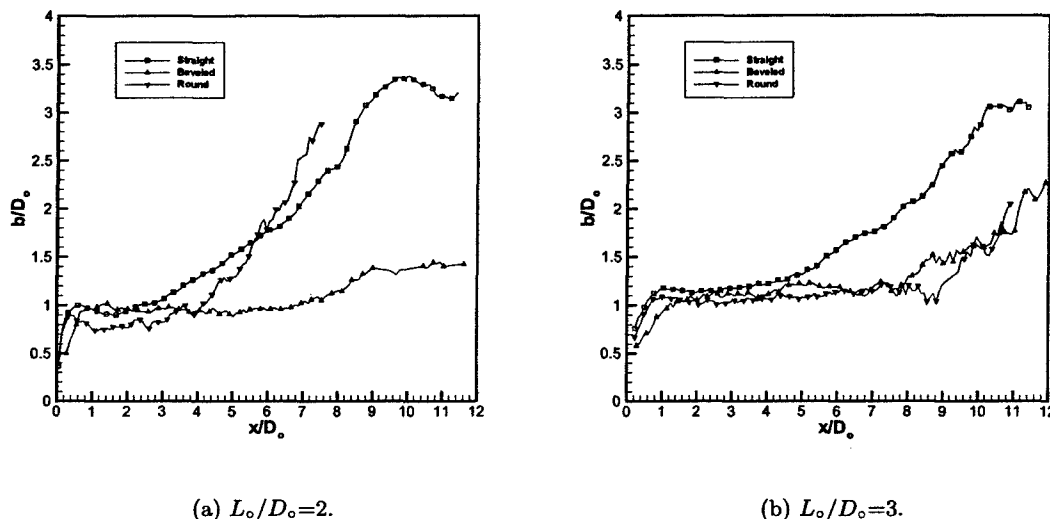

(a) $L_o/D_o=2$.   (b) $L_o/D_o=3$.

Figure 16: Comparison of the jet width for the straight, beveled, and round orifice. $Re_{U_o}=2500$.

4 INEEL Experimental Results

The interaction between a synthetic jet and a cross-flow boundary layer was studied for two synthetic jet orifice configurations, straight and 30° inclined. For both orifices, PIV measurements were obtained at $L_o/D_o = 1.0$ and 2.0 at $Re_{U_o}=250$. In the cross-flow, the freestream velocity was set to give an approximate velocity ratio, U_o/U_∞, of unity. At each of the actuator operating conditions, phase-averaged and asynchronous measurements were made.

4.1 Synthetic Jet from a Straight Orifice in a Cross-Flow

4.1.1 Phase-averaged flow field

Contours of the spanwise vorticity component, ω_z, with an overlay of velocity vectors are presented in Figure 17 at four phase angles for the straight orifice. In this figure, $L_o/D_o=1.0$. In this sequence, we see the formation of the vortex ring at the orifice during the expulsion portion of the actuator cycle ($\phi < 180°$). During the formation, the boundary layer separates

16

just upstream of the orifice, flowing up and over the forming vortex ring. In the cross-flow, the boundary layer is laminar, and it appears from the concentrations of positive vorticity in the separated flow that the Kelvin-Helmholtz instability is present in the shear layer. During the suction portion of the cycle, fluid from the upstream boundary layer, which is being drawn into the orifice, and the separated shear layer envelope the formation vortex ring diminishing the concentration of vorticity on the upstream portion of the ring. Note that during the suction portion of the cycle, fluid appears to be drawn into the orifice from upstream and downstream of the orifice. Late in the actuator cycle ($\phi \geq 306°$), the vorticity marking the upstream portion of the formation vortex ring is no longer evident; the downstream portion of the vortex ring is stationary near the downstream edge of the orifice where it slowly decreases in strength before merging with the vorticity in the separated boundary layer during the expulsion portion of the next actuator cycle. The effect of the forming vortex ring is to block the boundary layer flow in the vicinity of the orifice. An attached boundary layer still appears to exist downstream of the orifice, and between this boundary layer and the separated boundary layer from upstream of the orifice, there exists a weak wake-like region.

At the higher value of the stroke (L_o/D_o=2.0), the flow pattern is decidedly different (Figure 18). The forming vortex ring appears to completely block the boundary layer flow causing it to divert around and to get wrapped into the ring. The vortex ring does not appear to be forming symmetrically with respect to the axis of the orifice, and vorticity from the boundary layer downstream of the orifice obscures the downstream portion of the ring. Near the end of the expulsion portion of the actuator cycle, the forming vortex ring has penetrated to a height of $1.5D_o$ directly above the orifice. The initiation of the suction portion of the cycle detaches the ring from the orifice. At $\phi = 234°$, the induced motion at the wall from the vortex ring appears to have created a small region, about one orifice diameter in extent, of separated flow. It is interesting to note that during suction, fluid appears to be drawn primarily from the upstream boundary layer. Clearly, without the vortex ring shielding the orifice from the upstream boundary layer, the actuator draws less fluid from the downstream side. As the next actuator cycle begins, the vortex ring penetrates deep into the cross-flow, reaching a height in excess of three orifice diameters.

4.1.2 Mean flow field

The integrated effect of the time dependent behavior on the mean flow is shown in Figure 19 for L_o/D_o=1.0. The local blocking of the boundary layer at the actuator orifice is readily apparent with a region of reduced velocity extending to approximately $4D_o$ downstream. Beyond x/D_o=4.0, it appears that the velocity profile in the boundary layer is fuller than the upstream profile, a consequence perhaps of the reorientation of boundary layer vorticity in the flow outside of the measurement plane. In the mean, the flow at the orifice also pushes the boundary layer edge away from the wall by approximately $0.4D_o$. Above the boundary layer, there is a region of the freestream that appears to have accelerated as the flow passes over the boundary layer actuator interaction.
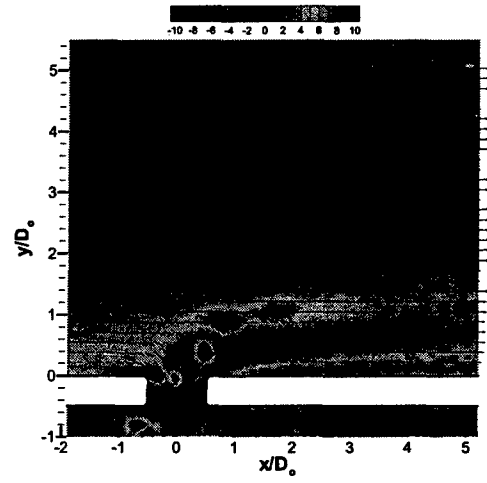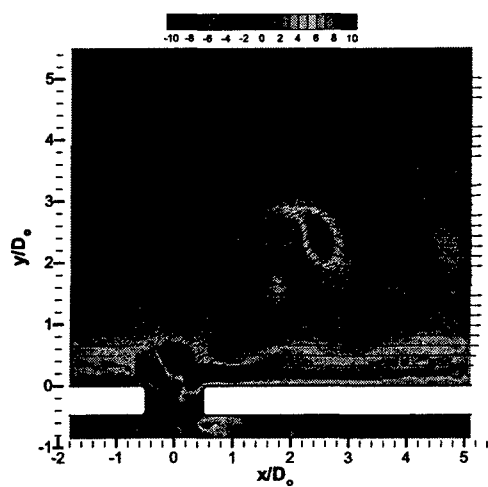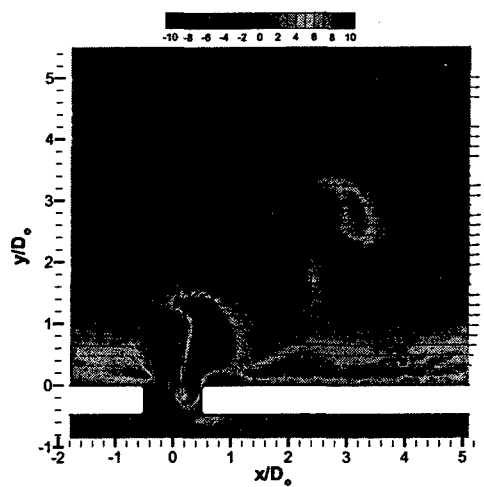
(a) $\phi = 72°$
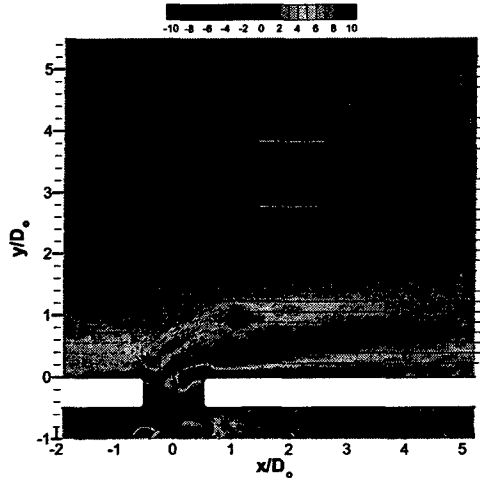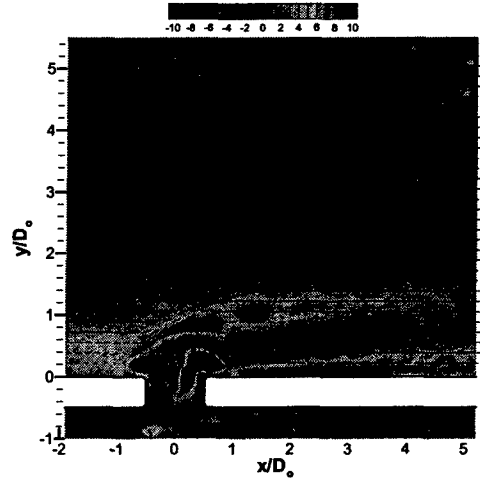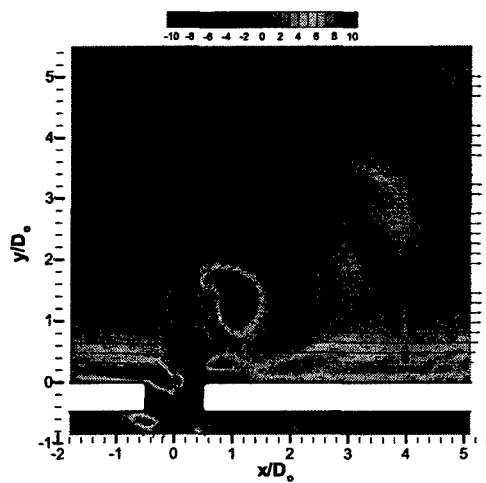
(b) $\phi = 162°$
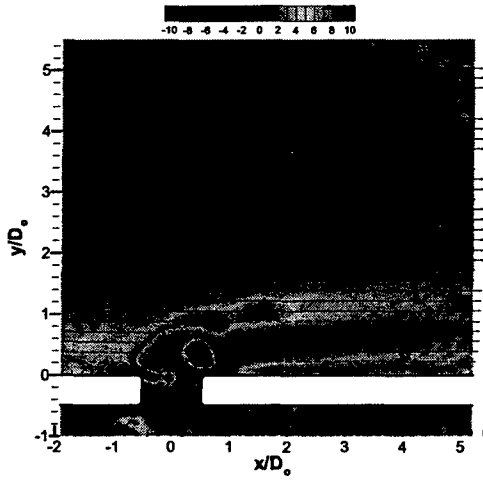
(c) $\phi = 234°$

(d) $\phi = 306°$

Figure 17: Contours of spanwise vorticity, ω_z, for the phase-averaged measurements of the straight orifice, $L_o/D_o = 1.0$.

(a) $\phi = 72°$

(b) $\phi = 162°$

(c) $\phi = 234°$

(d) $\phi = 306°$

Figure 18: Contours of spanwise vorticity, ω_z, for the phase-averaged measurements of the straight orifice, L_o/D_o=2.0.
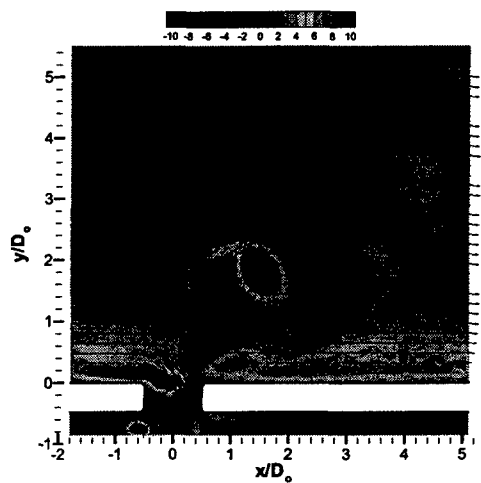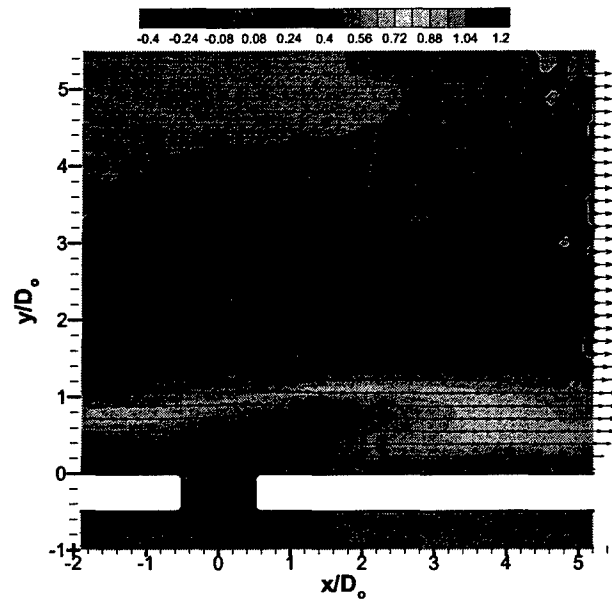
Figure 19: Contours of the mean streamwise velocity with an overlay of velocity vectors for the straight orifice at $L_o/D_o=1.0$.
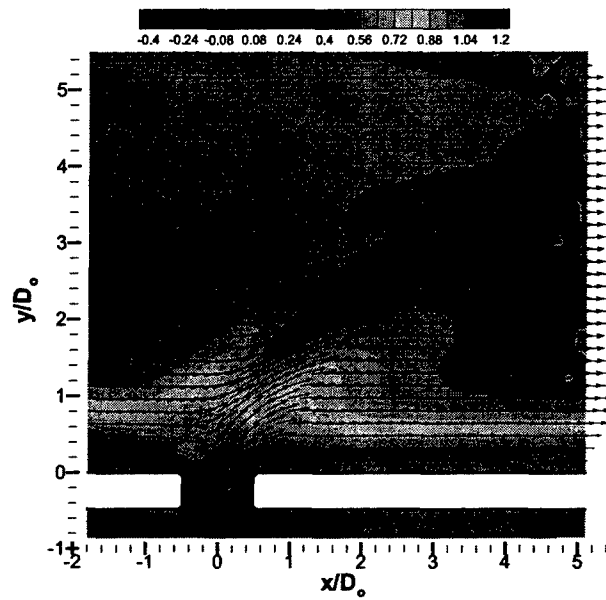

Figure 20: Contours of the mean streamwise velocity with an overlay of velocity vectors for the straight orifice at $L_o/D_o=2.0$.

20

At $L_o/D_o=2.0$ (Figure 20), the influence of the actuator is more localized in the streamwise direction. At this stroke, it is clear that, on average, the flow penetrates much deeper into the cross-flow and well beyond the edge of the boundary layer. The influence of the flow at the orifice appears to be confined to no more than $3D_o$ downstream, and here again, farther downstream, the boundary layer velocity profile appears to be fuller than the upstream profile.

4.2 Synthetic Jet from a 30° Inclined Orifice in a Cross-flow

4.2.1 Phase-averaged flow field

For the same actuator operating conditions ($L_o/D_o=1.0$, $Re_{U_o}=250$) inclining the axis of the orifice downstream at 30° to the vertical leads to a dramatic change in the flow (Figure 21) by comparison with the straight orifice (Figure 17). Flow separating from the downstream inside edge of the orifice causes the vortex ring to form in the upstream half of the orifice with a smaller diameter. While the ring is still forming, it begins to rotate counter-clockwise, and the rotation continues throughout the actuator cycle. As the next actuator cycle begins, the vortex ring convects downstream without much additional rotation. The downstream portion of the vortex ring is still evident at $x/D_o=5.0$ downstream of the orifice, but the upstream portion of the ring is not apparent beyond $x/D_o=3.0$. Unlike the vortex ring formed at the straight orifice, the vortex ring formed at the inclined orifice has moved sufficiently far away from the orifice by the beginning of the suction portion of the cycle not to block the orifice. Consequently, fluid appears to be drawn preferentially from the upstream side of the orifice during suction.

At $L_o/D_o=2.0$ (Figure 22), the vortex ring forming during the expulsion portion of the cycle appears to block the boundary layer flow causing a deceleration of the boundary layer upstream of the orifice. Downstream of the orifice, though, there appears to be an acceleration of the flow near the wall (Figure 22a). As the actuator cycle progresses, the downstream portion of the forming vortex ring entrains fluid from the boundary layer downstream of the orifice, and creates a region of separated flow immediately downstream of the orifice, extending more than one orifice diameter downstream. As the vortex ring convects into the cross-flow and away from the orifice, a region of fluid, identifiable by significant vertical velocity component, follows the vortex ring drawing low momentum fluid away from the wall as it moves. As was observed at $L_o/D_o=1.0$ during the suction portion of the actuator cycle, fluid is drawn preferentially from the boundary layer upstream of the orifice.

4.2.2 Mean flow field

By inclining the orifice downstream, the wall normal and streamwise extents of the boundary layer affected by the actuator flow when $L_o/D_o=1.0$ (Figure 23) are increased significantly by comparison to the straight orifice (Figure 19). The interaction extends to nearly $2D_o$ above the wall, and in the streamwise direction, the interaction reaches beyond $5D_o$. The local acceleration of the freestream observed for the straight orifice is also seen here, but starts farther downstream. The mean velocity vectors reveal a clear deflection of the flow away from the wall.
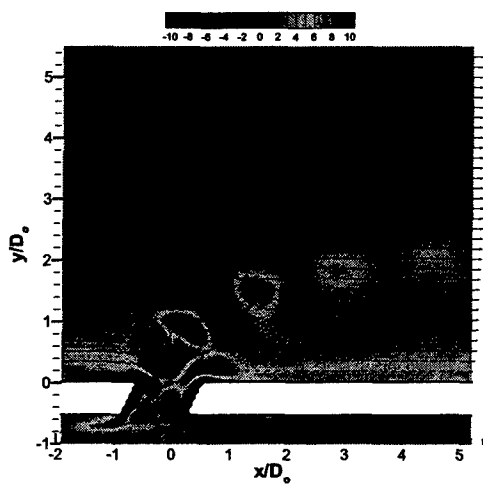
At $L_o/D_o=2.0$ (Figure 24), the mean interaction is confined primarily to the boundary layer
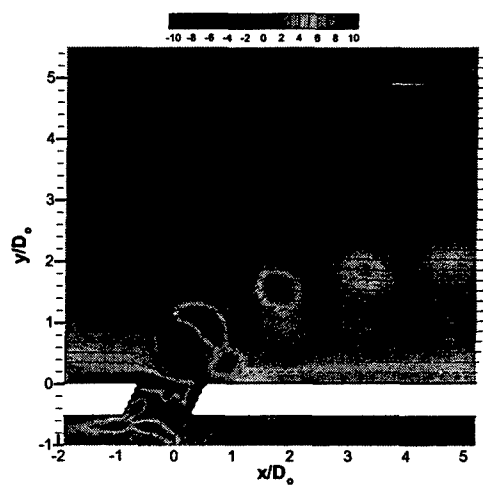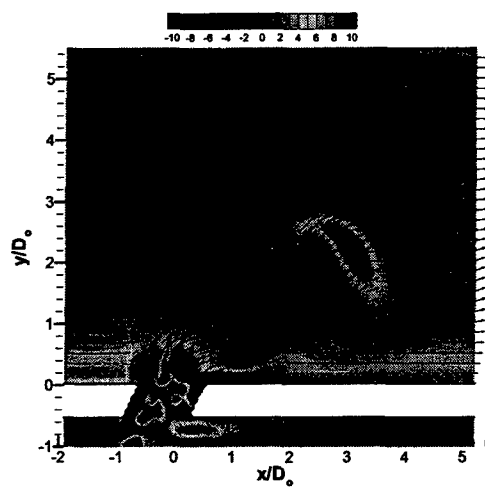
21

(a) $\phi = 72°$
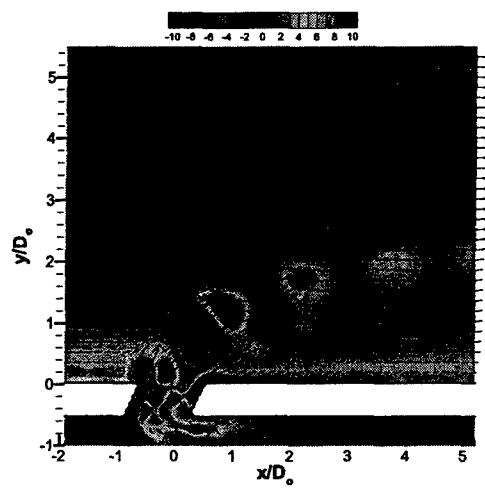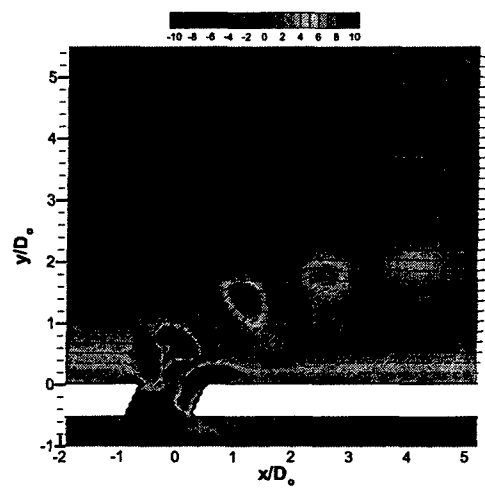
(b) $\phi = 162°$

(c) $\phi = 234°$

(d) $\phi = 306°$

Figure 21: Contours of spanwise vorticity, ω_z, for the phase-averaged measurements of the inclined orifice, $L_o/D_o = 1.0$.

(a) $\phi = 72°$

(b) $\phi = 162°$

(c) $\phi = 234°$
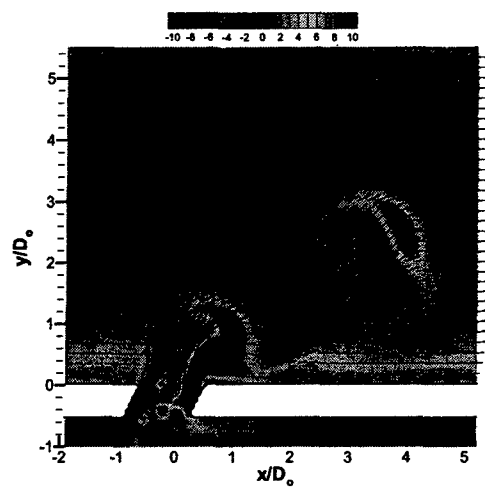

(d) $\phi = 306°$

Figure 22: Contours of spanwise vorticity, ω_z, for the phase-averaged measurements of the inclined orifice, $L_o/D_o = 2.0$.
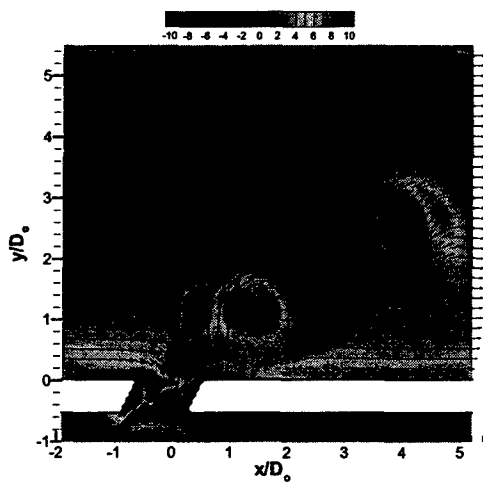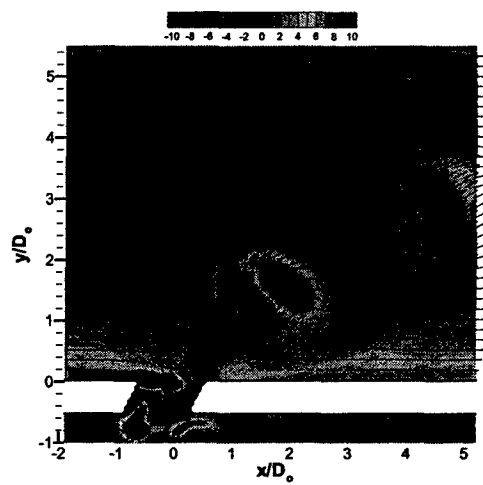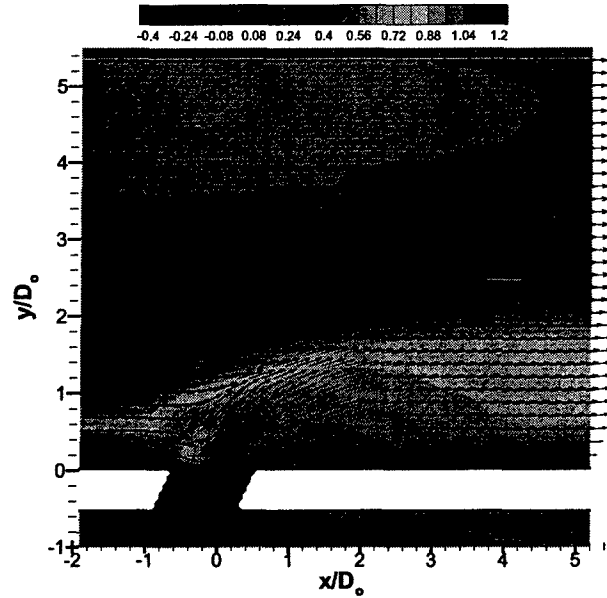
Figure 23: Contours of the mean streamwise velocity with an overlay of velocity vectors for the inclined orifice at $L_o/D_o=1.0$.

downstream of the orifice, and extends to approximately $4D_o$ downstream. In the wall normal direction, the interaction reaches to $y = 2D_o$. In contrast to the straight orifice, the deflection of the flow is larger in the wall normal direction and persists farther downstream.

5   Summary Discussion

The two objectives of this work were to examine the scaling of an axisymmetric synthetic jet in the context of scaling for vortex ring formation (Gharib et al. 1998), and to investigate the interaction of a synthetic jet with a cross-flow boundary layer.

From the synthetic jet scaling experiments, the role of actuator stroke, Reynolds number, and orifice lip shape on the synthetic jet formation were assessed. The actuator stroke, expressed as L_o/D_o, appears to play the defining role in synthetic jet formation; the value of the stroke determines how far from the orifice the vortex rings will convect downstream before they begin to be distorted in the transition to a synthetic jet. Once a synthetic jet is formed, the mean flow properties appear to scale well on the slug flow model velocity, U_o, and the mean flow behavior, for example the width of the synthetic jet, appears to be independent of Reynolds number. The shape of the orifice lip also plays an important role in the character of the flow formed at the actuator orifice. A synthetic jet formed close to the orifice was only observed for the straight orifice configuration. For the round and beveled orifices, the actuator flow most closely resembled a train of vortex rings.

For the experiments examining the interaction of a synthetic jet and a cross-flow boundary layer,
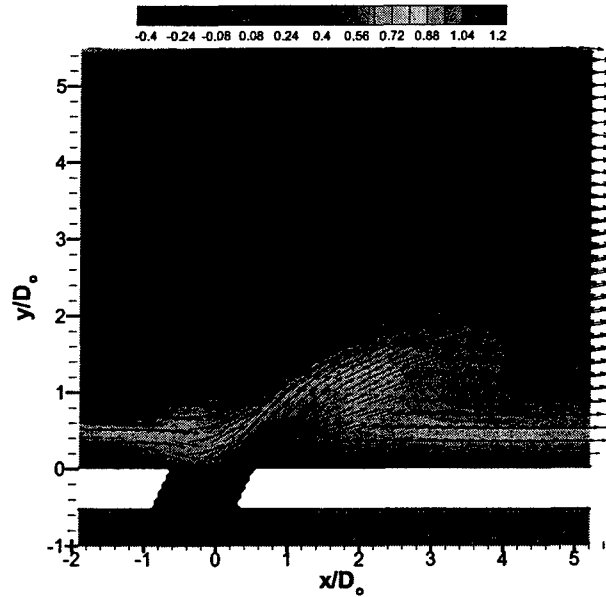
24

Figure 24: Contours of the mean streamwise velocity with an overlay of velocity vectors for the inclined orifice at $L_o/D_o=2.0$.

the actuator stroke and inclination of the orifice, relative to the vertical, were important to the character of the interaction. Two values of the stroke, L_o/D_o, were investigated, 1.0 and 2.0. At $L_o/D_o=1.0$ and for both orifice orientations, the actuator flow blocks the incoming boundary layer, leading to a wake-like region that extends 3-5D_o downstream of the orifice. At the higher stroke ($L_o/D_o=2.0$), the boundary layer interaction is confined to the immediate vicinity of the orifice, as the actuator flow rapidly penetrates beyond the boundary layer edge and into the freestream fluid. In the four cases studied, only at the low stroke for the vertical orifice did the actuator draw fluid from upstream and downstream of the orifice during the suction portion of the actuator cycle. In the other three cases, the fluid was drawn preferentially from the upstream boundary layer flow. For the vertical orifice, the boundary layer downstream of the interaction appeared to be thinner than the upstream boundary layer perhaps as a result of high momentum fluid being drawn into the wake-like region behind the interaction. For the inclined orifice, no apparent change in the boundary layer thickness was observed.

The results of the cross-flow experiments are particularly interesting and elucidating, and as a recommendation for future work, additional work looking at cross-span views of the interaction and obtaining measurements in planes parallel to the orifice plane would be extremely useful in understanding the interaction of the synthetic jet and boundary layer. In addition, measurements of this type would provide important comparisons for studies engaged in numerical modeling and prediction of synthetic jet flows.

6 Personnel Supported

Jennifer Shuster	Graduate Student, M.S. 2005, University of Wyoming
Douglas R. Smith	Assciate Professor, University of Wyoming
Donald McEligot	Technical Leader, Idaho National Engineering and Environment Laboratory
Robert J. Pink	Idaho National Engineering and Environment Laboratory

7 Publications From This Work

Shuster, J. M. and Smith, D. R., "A Study of the Formation and Scaling of a Synthetic Jet", AIAA Paper 2004-0090, AIAA 42nd Aerospace Sciences Meeting, Reno, NV, January 2004.

Shuster, J. M., Pink, R. J., McEligot, D. M. and Smith, D. R., "The Interaction of a Circular Synthetic Jet with a Cross-flow Boundary Layer", AIAA Paper 2005-4749, To be presented at the 35th AIAA Fluid Dynamics Conference, Toronto, Ontario, Canada, 6–9 June 2005.

Shuster, J. M. and Smith, D. R., "The Effect of Orifice Size and Lip Shape on the Formation of a Synthetic Jet", AIAA Paper 2005-4750, To be presented the 35th AIAA Fluid Dynamics Conference, Toronto, Ontario, Canada, 6–9 June 2005.

8 AFRL Points of Contact

Carl Tillmann	Air Vehicles Directorate
Greg Addington	Air Vehicles Directorate

References

Amitay, M., D. R. Smith, V. Kibens, D. E. Parekh, and A. Glezer (2001). Aerodynamic flow control over an unconventional airfoil using synthetic jet actuators. *AIAA Journal 39*(3), 361–370.

Gharib, M., E. Rambod, and K. Shariff (1998). A universal time scale for vortex ring formation. *Journal of Fluid Mechanics 360*, 121–140.

Glezer, A. (1988). The formation of vortex rings. *Physics of Fluids 31*(12), 3532–3542.

Smith, B. L. and A. Glezer (2002). Jet vectoring using synthetic jets. *Journal of Fluid Mechanics 458*, 1–34.

Smith, B. L., M. A. Trautman, and A. Glezer (1999). Controlled interactions of adjacent synthetic jet actuators. AIAA Paper 99-0669, AIAA 37th Aerospace Sciences Mtg., Reno, NV, January 11-14, 1999.